2.3 Fabrication and Characterization of Oriented Fe-$Y_2Ti_2O_7$ Interfaces: Implications to the Development and Optimization of Nanostructured Ferritic Alloys — T. Stan, Y. Wu and G. R. Odette (University of California Santa Barbara), K. Sickafus (University of Tennessee), H. Dabkowska and B. Gaulin (McMaster University)

OBJECTIVE

The objective of this work is to better understand and characterize the interfaces between Y-Ti-O nano-features (NFs) and the bcc Fe-Cr ferrite matrix in nanostructured ferritic alloys (NFA).

SUMMARY

The smallest 2-3 nm features in NFA are $Y_2Ti_2O_7$ complex oxide cubic pyrochlore phase. The interface between the bcc Fe-Cr ferrite matrix and the fcc $Y_2Ti_2O_7$ plays a critical role in the stability, strength and damage tolerance of NFA. To complement other characterization studies of the actual embedded nano-features, a mesoscopic interface was created by electron beam deposition of a thin Fe layer on a {111} $Y_2Ti_2O_7$ bulk single crystal surface. We recognize that the mesoscopic interfaces may differ from those of the embedded NFs, but the former will facilitate characterization and investigations of the functionality of controlled interfaces, such as interactions with point defects and helium. The Fe-$Y_2Ti_2O_7$ interface was characterized using scanning electron microscopy (SEM), including electron back scattering diffraction (EBSD), atomic force microscopy (AFM), X-ray diffraction (XRD), and transmission electron microscopy (TEM). The polycrystalline Fe layer has two general orientation relationships (OR) that are close to: a) $(110)_{Fe}||(111)_{Y2Ti2O7}$ and $[001]_{Fe}||[1\text{-}10]_{Y2Ti2O7}$ [notably, this is a Nishiyama-Wasserman (NY) OR]; b) $(001)_{Fe}||(111)_{Y2Ti2O7}$ and $[100]_{Fe}||[1\text{-}10]_{Y2Ti2O7}$. High resolution TEM was used to characterize details of the interfaces, which ranged from being atomically sharp, with interface defects, to those with more diffuse interface zones that, in some cases, included a thin FeO_x layer.

PROGRESS AND STATUS

Background

Materials in fission and fusion reactor environments are subject to high temperatures, large time-varying stress, chemically reactive environments, and intense radiation fields [1]. Helium that is produced by transmutation reactions interacts with displacement damage to drive complex microstructural evolutions. Most notably, helium is insoluble in steels and precipitates as gas bubbles that act as formation sites for both growing voids and creep cavities, while helium also weakens grain boundaries over a wide range of temperatures. NFA have been found to be radiation tolerant since they contain an ultrahigh density of Y-Ti-O NFs that trap helium in harmless, fine-scale bubbles, suppressing void swelling and embrittlement. NFs also provide high stable sink densities for defect annihilation and high creep strength due to dislocation pinning [2].

Most previous TEM studies have indicated that the NFs are complex oxides, primarily fcc cubic pyrochlore $Y_2Ti_2O_7$. For example, scanning transmission electron microscopy (STEM) energy dispersive X-ray (EDX) measurements on NF extracted from NFA MA957, reported by

Sakasegawa et al., indicate that they are non-stiochiometric $Y_2Ti_2O_7$, with Y/Ti < 1.0 for precipitates in the larger size range up to 15 nm and Y/Ti ≈ 0.5 for the smallest pyrochlore features [3]. At largest sizes, from ≈ 15 to 35 nm, the oxides are closer to stiochiometric, with Y/Ti ≈ 1.0. Yamashita et al. also found non-stiochiometric $Y_2Ti_2O_7$, but generally with a range of Y/Ti slightly greater than 1 [4,5]. Klimiankou et al. found near stoichiometric $Y_2Ti_2O_7$ in a 9Cr NFA using electron energy loss spectroscopy, HRTEM-fast Fourier transform (FFT) power spectra indexing and energy filtered TEM (EFTEM) methods [6,7]. Early x-ray diffraction (XRD) studies by Okuda and Fujiwara also indicated the presence of $Y_2Ti_2O_7$ in a 14Cr model NFA [8]. This observation has been confirmed by Sasasegawa et al. based on XRD measurements of nanopore filtered oxides extracted from a 9 Cr martensitic alloy [8]. Recently, Yu et al. reported a comprehensive TEM characterization study of NFA MA957 in different conditions, using various techniques [9]. This work clearly showed that extracted NFs are structurally consistent with $Y_2Ti_2O_7$ and generally are near stoichiometric with Y/Ti ratios from 0.5 to 1. The dominant in-foil interface was found to be parallel to the {100} planes in Fe, although the oxide themselves could not be indexed. Note Yu also discusses some other recent work in the literature that did not find the pyrochlore yttrium titanate. Finally, a recent high resolution TEM (HRTEM) study by Cisten et al. confirmed that the in-foil NFs in the same friction stirred weld variant of MA957 are $Y_2Ti_2O_7$ [10]. The study on the TEAM 0.5 microscope at LBL showed that the dominant NF in-foil interface OR is $(100)_{Matrix}||(100)_{Y2Ti2O7}$ and $[001]_{matrix}||[1\text{-}10]_{Y2Ti2O7}$.

The high density of NFs trap He in fine bubbles [11] and pin dislocations. The NFs are also remarkably thermally stable [12,13]. However, the details of important processes (mechanisms and energies), such as helium trapping, are not well understood. Thus, while they may differ from those for embedded NFs, creating a variety of mesoscopic surrogates, with self-selected sets of ORs with bcc Fe, will facilitate developing a general understanding of such metal-oxide interfaces in NFA, especially with respect to their structures and functional properties.

Experimental Methods

A pure single crystal of $Y_2Ti_2O_7$ was acquired from McMaster University (Dabkowska and Gaulin). The crystal was grown using a two-mirror NEC floating zone image furnace. The starting materials for the polycrystalline rods were 99.999% pure Y_2O_3 and 99.995% pure TiO_2, both from Alfa Aesar. The feed rods were created in the same fashion as Gardner [14]. The final single crystal was grown using the floating zone technique at a speed 5 mm/hr in air [15]. A 1.8 mm wafer was cut with a diamond saw parallel to the $Y_2Ti_2O_7$ single crystal {111} surface. An Allied Multiprep system was used to polish the wafer using a sequence of 15 (for flattening), 9, 6, 3, 1, 0.5 and 0.1 μm papers for 10 minutes each at 75 rpm. The final 15 minute polishing step used a 0.02 μm non-crystallizing silica suspension.

An electron beam system was used to deposit Fe on the $Y_2Ti_2O_7$ crystal at 7×10^{-6} torr and 800°C. The deposition rate was 0.3 nm/s for 420 s, producing a total Fe layer thickness of ≈ 200 nm. The sample was then slowly cooled to room temperature at a rate of ≈ 0.16°C/s.

Results and Discussion

Deposits of Fe on a pyrex glass substrate were used to provide a naturally selected Fe grain OR for an amorphous control surface. AFM measurements show the deposit is characterized by many Fe polycrystals with average grain size of 1 μm and a surface roughness of about 40 nm (Figure 1a). XRD scans show that the grains have a {110} out-of-plane pole orientation.

The XRD <100>$_{Fe}$ pole figure forms a ring showing that, as expected, there is no in-plane orientation between the Fe polycrystals and the pyrex glass (Figure 1b). The same deposition conditions were used for the $Y_2Ti_2O_7$ {111} oriented substrate.

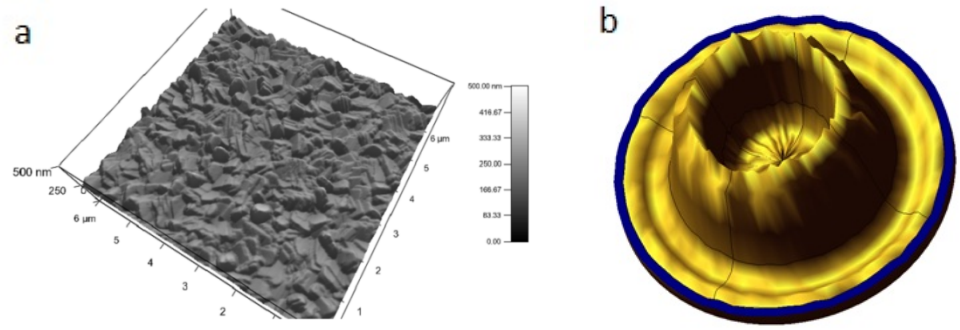

Figure 1. (a) AFM 3D reconstruction of the Fe grains on Pyrex. (b) Pole figure showing no in-plane OR between the Fe grains and the Pyrex.

The SEM image in Figure 2a shows a polycrystalline layer of Fe on the (111) $Y_2Ti_2O_7$ surface, with average grain size of about 1 µm, similar to that found in the pyrex control sample. The corresponding EBSD inverse pole map in Figure 2b and pole figures in Figure 2c show that the Fe grains have two orientations with the $\{111\}_{Y2Ti2O7}$ surface parallel to Fe grains with both $\{100\}_{Fe}$ and $\{110\}_{Fe}$. No $\{111\}_{Fe}$ grains were observed.

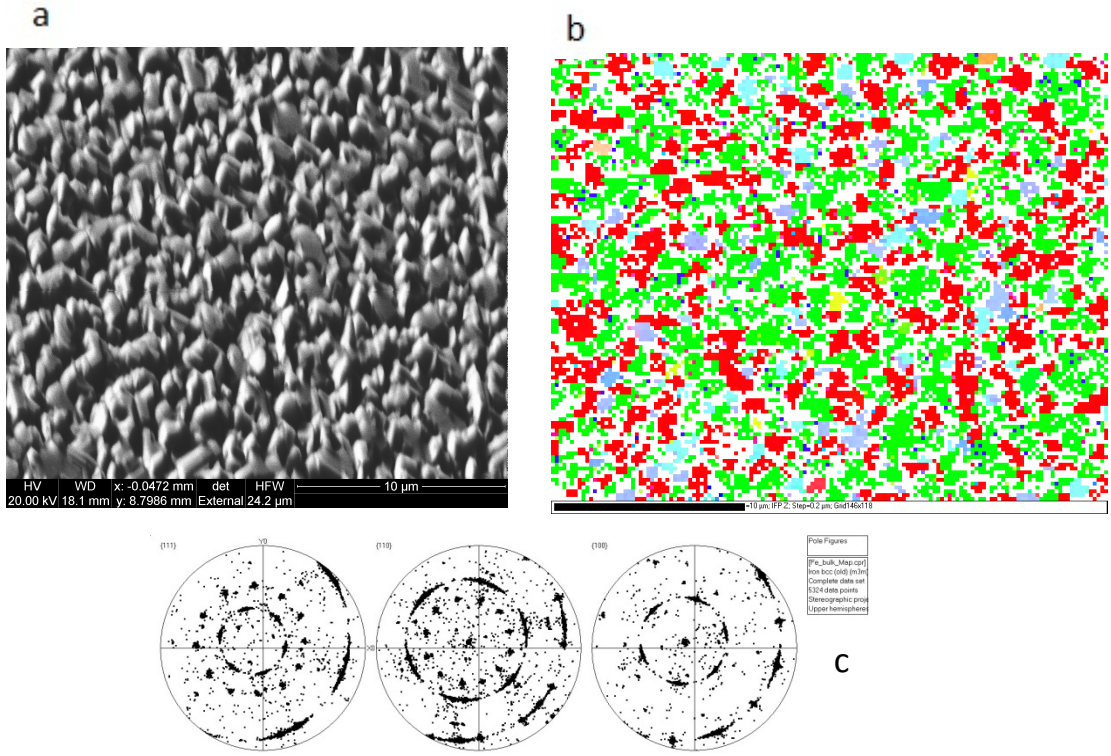

Figure 2. (a) EBSD of Fe grains on the $Y_2Ti_2O_7$ single crystal substrate. (b) Inverse pole figure map of the Fe grains. $\{100\}_{Fe}$ in red and $\{110\}_{Fe}$ in green. (c) Pole figures of Fe on $Y_2Ti_2O_7$. No $\{111\}_{Fe}$ grains, but many grains with $\{110\}_{Fe}$ and $\{100\}_{Fe}$.

The XRD scan in Figure 3 confirms the surface ORs observed with EBSD. T he $\{111\}_{Y2Ti2O7}$ is parallel to $\{110\}_{Fe}$ and to $\{100\}_{Fe}$.

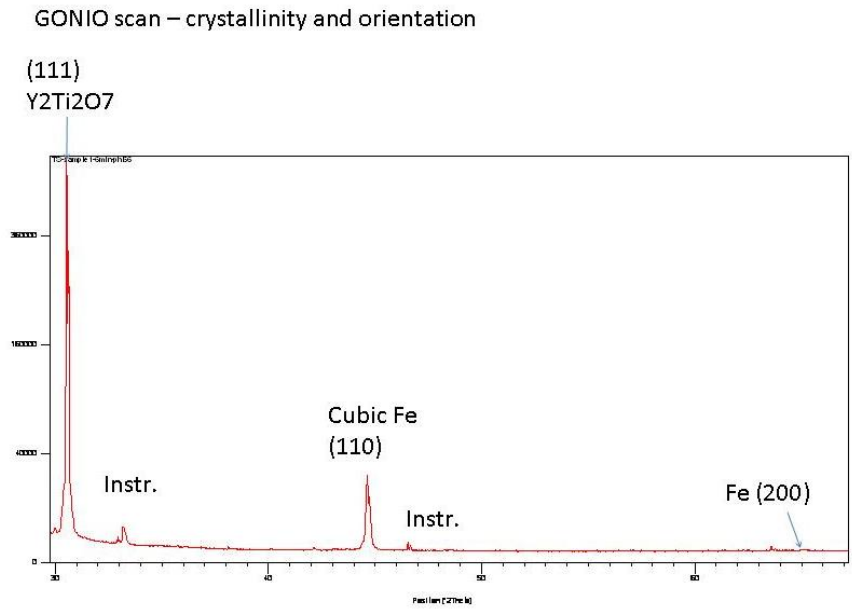

Figure 3. XRD of the Fe grains on the $Y_2Ti_2O_7$ substrate showing the $\{111\}_{Y2Ti2O7}$ reflection, the $\{110\}_{Fe}$ reflection, and a weak $\{200\}_{Fe}$ reflection. Signals are also seen from the XRD stage.

The XRD pole measurements in Figure 4 also show that there are two in-plane ORs: $<110>_{Y2Ti2O7}$ parallel to $<100>_{Fe}$ and to $<111>_{Fe}$. This further demonstrates that the $Y_2Ti_2O_7$ substrate affects the orientation of the Fe grains that grew during deposition.

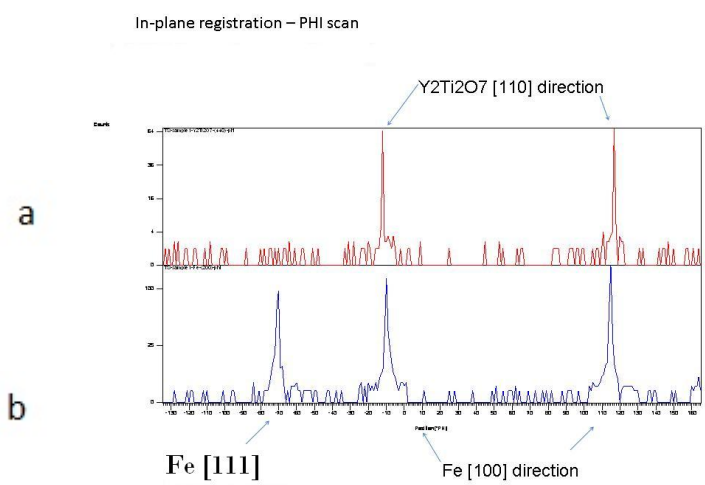

Figure 4. (a) The <110> in-plane direction of the $Y_2Ti_2O_7$ substrate. (b) The Fe in-plane directions. The Fe <100> peaks line up with the $Y_2Ti_2O_7$ <110> peaks. The $<111>_{Fe}$ reflection is also seen.

A FEI HELIOS Focused Ion Beam (FIB) tool was used to micro-machine < 20 nm thick electron transparent lift-outs of the interface as shown in Figure 6. The sample was cleaned by a low energy ion beam with 2 keV 5.5 pÅ. HRTEM, STEM and EDX were performed on the 300 keV FEI Titan TEM in the UCSB microstructure and microanalysis facility.

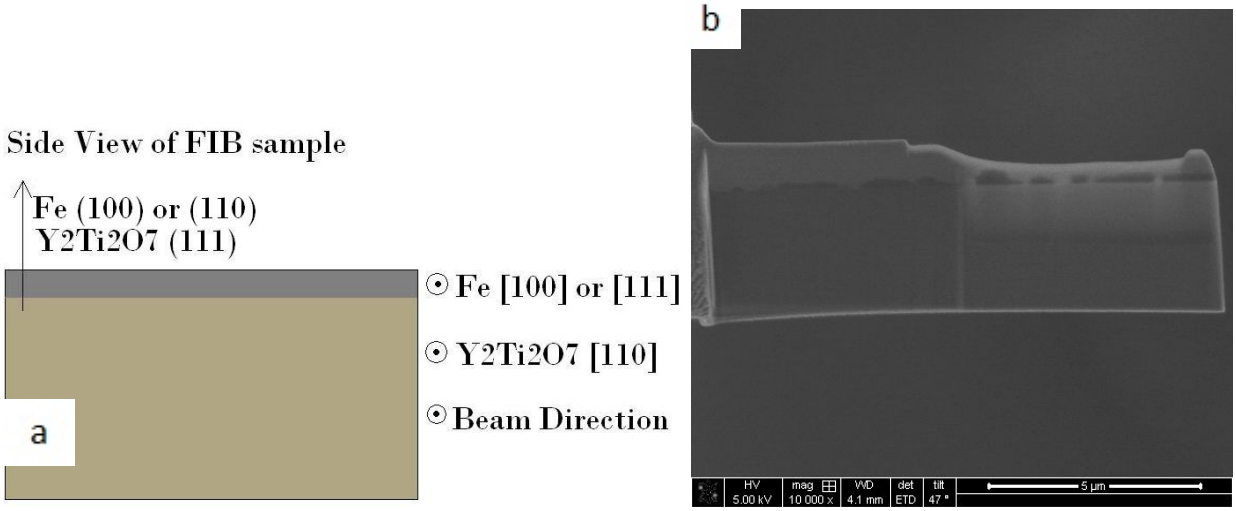

Figure 6. (a) Side view of FIB sample showing surface and direction ORs. (b) SEM image of the FIB sample used for TEM. The $<110>_{Y2Ti2O7}$ points out of the page.

TEM characterization

Figure 7 shows the low magnification TEM image of the cross-section of the lift out. A total of 13 grains were examined using TEM.

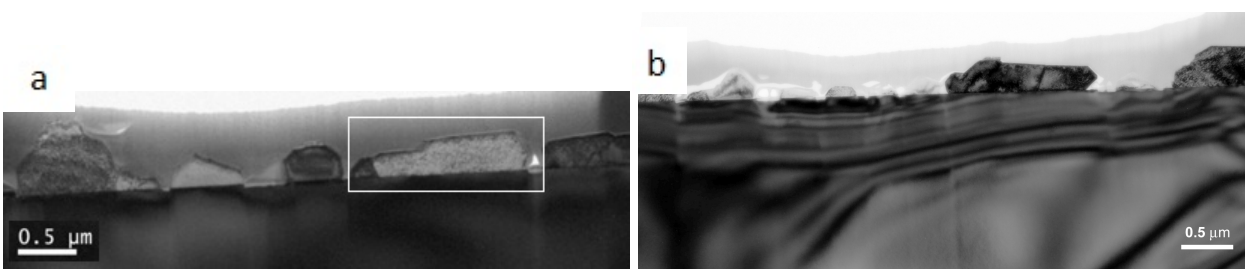

Figure 7. (a) and (b) are cross-section TEM images of Fe grains on the {111} $Y_2Ti_2O_7$ substrate. The white rectangle is enlarged for detail in Figure 8.

Six grains have an OR: $\{1\text{-}10\}_{Fe}||\{111\}_{Y2Ti2O7}$ and $<111>_{Fe}||<1\text{-}10>_{Y2Ti2O7}$ (off 5°-10°). Four grains have the OR: $\{001\}_{Fe}||\{111\}_{Y2Ti2O7}$ (off ~1°) and $<100>_{Fe}||<110>_{Y2Ti2O7}$; one grain has the OR: $\{110\}_{Fe}||\{111\}_{Y2Ti2O7}$ (off ~1°) and $<100>_{Fe}||<110>_{Y2Ti2O7}$; and 2 grains have no OR with the (111) $Y_2Ti_2O_7$ substrate. These results are summarized in Table 1.

Table 1. Summary of the OR found for the 13 grains observed with HRTEM.

Grain	Size	Orientation
No. 1	600 nm x 500 nm	$\{001\}_{Fe}$ ||$\{111\}_{Y2Ti2O7}$ $<111>_{Fe}$||$<1\text{-}10>_{Y2Ti2O7}$ (off 5°-10°)
No. 2	500 nm x 200 nm	No OR
No. 3	400 nm x 300 nm	$\{001\}_{Fe}$||$\{111\}_{Y2Ti2O7}$ (off ~1°) $<100>_{Fe}$||$<1\text{-}10>_{Y2Ti2O7}$
No. 4	250 nm x 200 nm	$\{001\}_{Fe}$||$\{111\}_{Y2Ti2O7}$ (off ~1°) $<100>_{Fe}$||$<1\text{-}10>_{Y2Ti2O7}$
No. 5	1000 nm x 300 nm	$\{1\text{-}10\}_{Fe}$||$\{111\}_{Y2Ti2O7}$ $<111>_{Fe}$||$<1\text{-}10>_{Y2Ti2O7}$ (off 5°-10°)
No. 6	1000 nm x 250 nm	$\{001\}_{Fe}$||$\{111\}_{Y2Ti2O7}$ (off ~1°) $<100>_{Fe}$||$<110>_{Y2Ti2O7}$
No. 7	1000 nm x 400 nm	$\{001\}_{Fe}$||$\{111\}_{Y2Ti2O7}$ $<001>_{Fe}$||$<1\text{-}10>_{Y2Ti2O7}$
No. 8	500 nm x 300 nm	$\{110\}_{Fe}$||$\{111\}_{Y2Ti2O7}$ $<001>_{Fe}$||$<1\text{-}10>_{Y2Ti2O7}$
No. 9	1000 nm x 500 nm	$\{1\text{-}10\}_{Fe}$||$\{111\}_{Y2Ti2O7}$ $<111>_{Fe}$||$<1\text{-}10>_{Y2Ti2O7}$ (off ~1°)
No. 10	1000 nm x 500 nm	$\{1\text{-}10\}_{Fe}$||$\{111\}_{Y2Ti2O7}$ $<111>_{Fe}$||$<1\text{-}10>_{Y2Ti2O7}$ (off 5°-10°)
No. 11	250 nm x 100 nm	$\{1\text{-}10\}_{Fe}$||$\{111\}_{Y2Ti2O7}$ $<111>_{Fe}$||$<1\text{-}10>_{Y2Ti2O7}$ (off 5°-10°)
No. 12	15 nm x 75 nm	$\{1\text{-}10\}_{Fe}$||$\{111\}_{Y2Ti2O7}$ $<111>_{Fe}$||$<1\text{-}10>_{Y2Ti2O7}$ (off 5°-10°)
No. 13	500 nm × 500 nm	No OR

The structure of the Fe-$Y_2Ti_2O_7$ Interface

The rectangular area in Figure 7 that is enlarged in Figure 8c shows two coalesced Fe grains with different orientations. Figure 8a shows the nano-diffraction pattern from the left grain, while Figure 8b shows the nano-diffraction pattern from the right grain. The left grain has an epitaxial relationship with the $Y_2Ti_2O_7$ substrate: $\{001\}_{Fe}$||$\{111\}_{Y2Ti2O7}$ and $<100>_{Fe}$||$<1\text{-}10>_{Y2Ti2O7}$. The right grain has the OR: $\{110\}_{Fe}$||$\{111\}_{Y2Ti2O7}$ and $<111>_{Fe}$||$<1\text{-}10>_{Y2Ti2O7}$ (off 5°-10°).

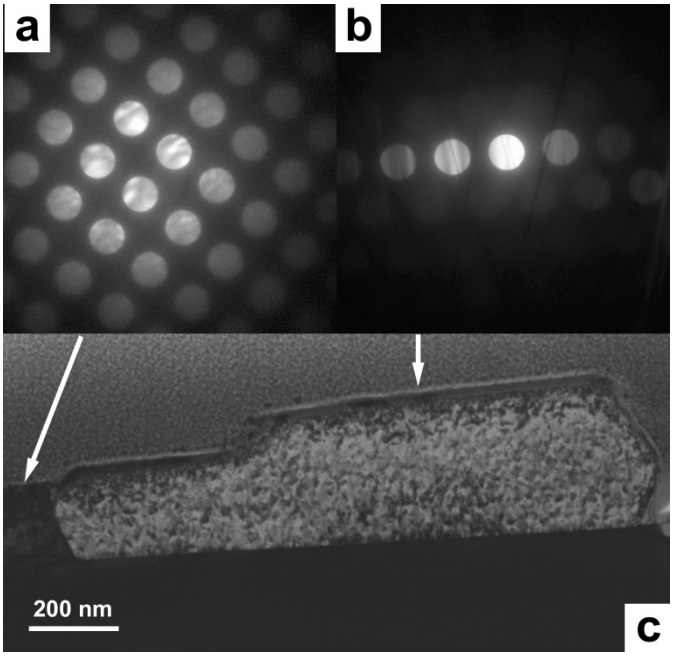

Figure 8. Nano diffraction patterns from the left grain and the right grain in (c) are shown in (a) and (b), respectively.

Figure 9 shows the interfacial structure of a grain with the OR: $\{1\text{-}10\}_{Fe}||\{111\}_{Y2Ti2O7}$ and $<111>||<1\text{-}10>_{Y2Ti2O7}$ (5°-10° off). This is close to the Kurdjamov-Sachs OR commonly found in fcc/bcc interfaces. The Fe-$Y_2Ti_2O_7$ interface has areas of dark and light patches spaced about 5 nm apart. The dark areas are stressed sections of the interface, which may be due to the miss cut of the $Y_2Ti_2O_7$ substrate.

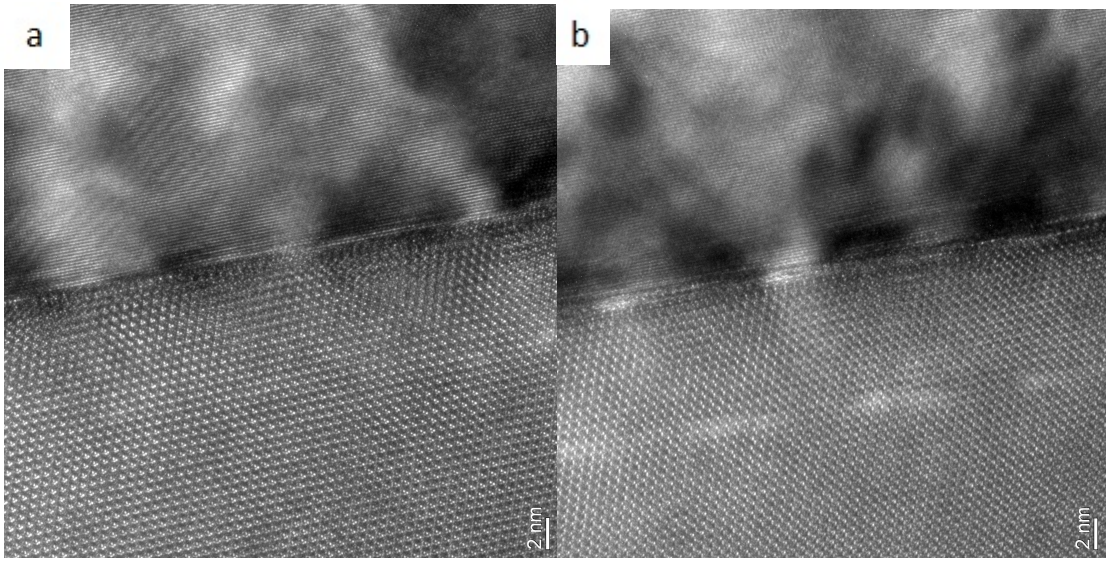

Figure 9. HRTEM images from a grain with $\{1\text{-}10\}_{Fe}||\{111\}_{Y2Ti2O7}$ and $<111>||<1\text{-}10>_{Y2Ti2O7}$ (5°-15° off) OR.

Figure 10 shows the HRTEM images for a grain with the OR: $\{001\}_{Fe}||\{111\}_{Y2Ti2O7}$ (off ~1°) and $<100>_{Fe}||<110>_{Y2Ti2O7}$. Figure 11 shows that the grains with this orientation have a 2-3 nm thick transition layer; and STEM/EDX showed the transition layer is rich in Ti, O and Fe.

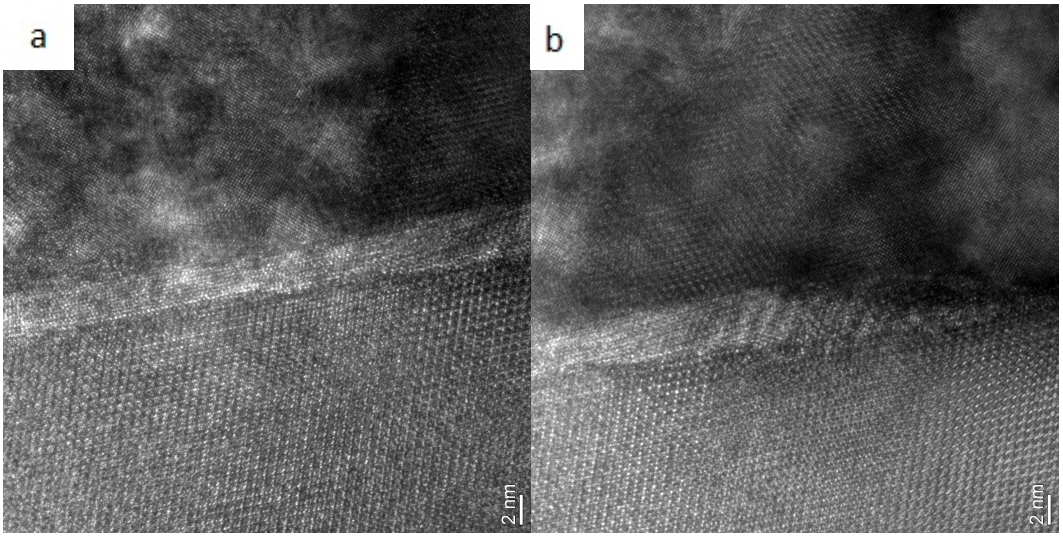

Figure 10. HRTEM images showing the light transitional layer found between Fe and $Y_2Ti_2O_7$ in the $\{001\}_{Fe}||\{111\}_{Y2Ti2O7}$ (off ~1°) and $<100>_{Fe}||<110>_{Y2Ti2O7}$ OR.

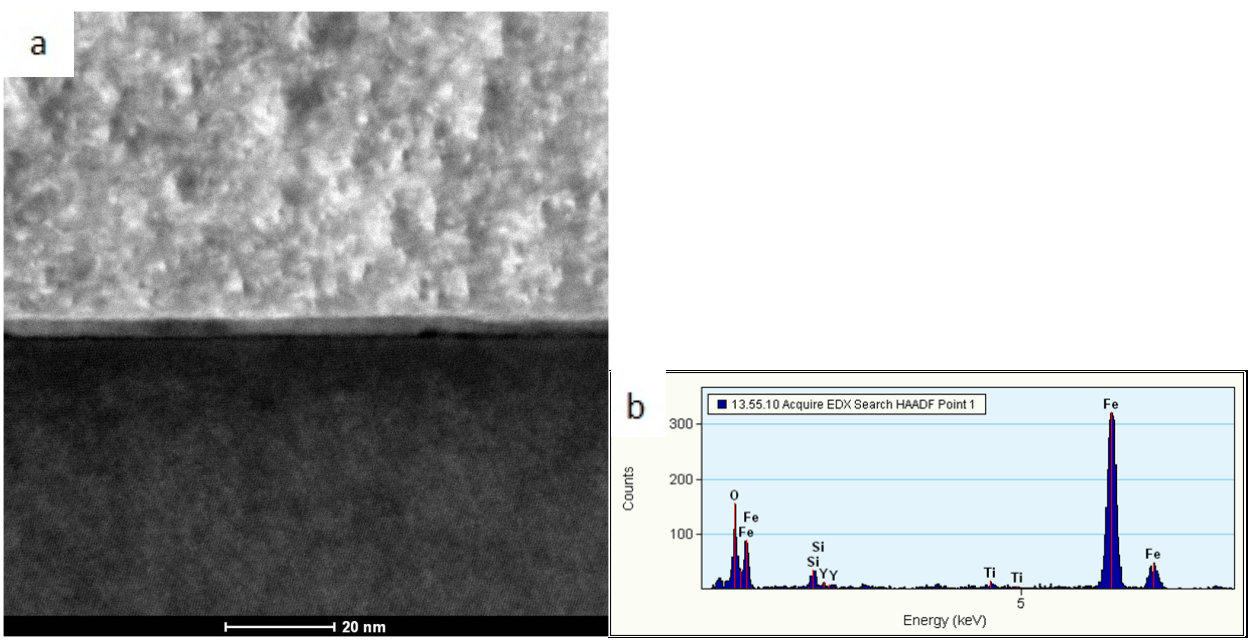

Figure 11. (a) STEM image of the $\{001\}_{Fe}||\{111\}_{Y2Ti2O7}$ (off ~1°) and $<100>_{Fe}||<110>_{Y2Ti2O7}$ OR. (b) an EDX spectra taken from the interfacial transition layer in image (a).

Figure 12a and 12b show a grain with no clear OR with the $Y_2Ti_2O_7$ substrate. The interface may be incoherent, and the dark area at the interface may again be a FeO_x transition layer.

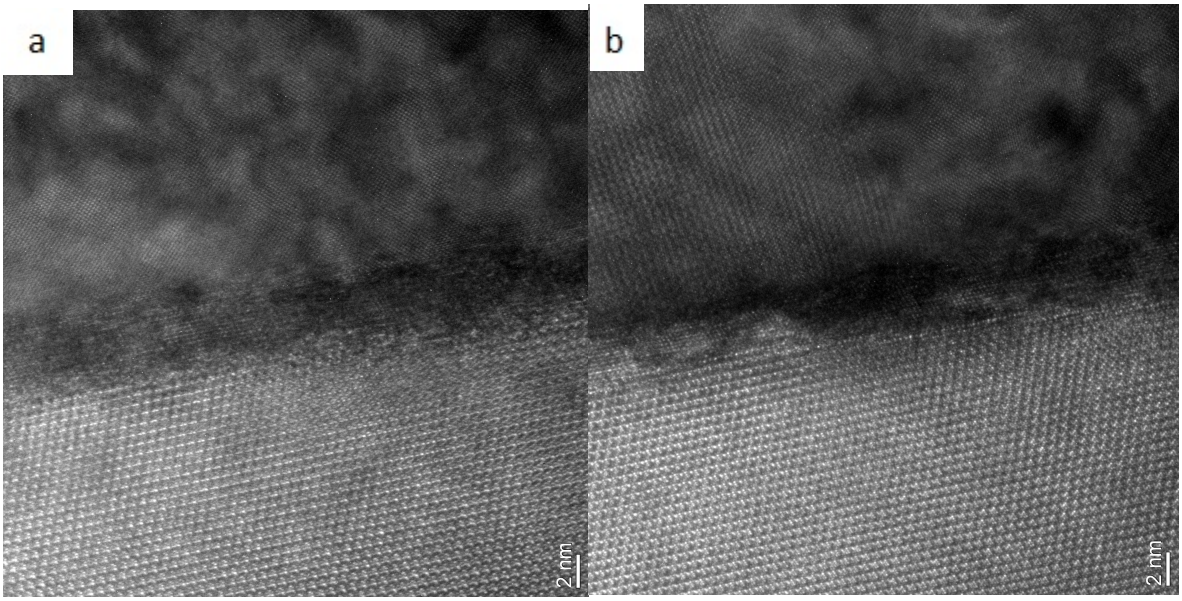

Figure 12. (a) and (b) show the interface of an Fe grain with no OR to the substrate.

CrystalMaker Studies of the Fe-$Y_2Ti_2O_7$ Interface

The $\{1\text{-}10\}_{Fe}||\{111\}_{Y2Ti2O7}$ and $<111>_{Fe}||<1\text{-}10>_{Y2Ti2O7}$ (off 5°-10°) OR was modeled with the CrystalMaker software (Figure 12a). The Kurdjumov-Sachs (KS) OR is obtained from the Nishiyama-Wasserman (NW) orientation by a 5.26˚ rotation about the interface normal [16]. The NW OR is $(110)_{Fe}||(111)_{Y2Ti2O7}$ and $[001]_{Fe}||[1\text{-}10]_{Y2Ti2O7}$. The $[001]_{Fe}$ and $[1\text{-}10]_{Y2Ti2O7}$ aligned direction mismatch is 2.5%. Note pattern of two well-matched Fe to substrate atoms (green) followed by a Fe defect location (purple) in Figure 12b. This calculation shows that there is a defect every 3 Fe <110> lengths, or 12.244 Å. Otherwise the interface is reasonably well matched. Note these calculations/images were made using the ideal unit cell parameters of the crystal.

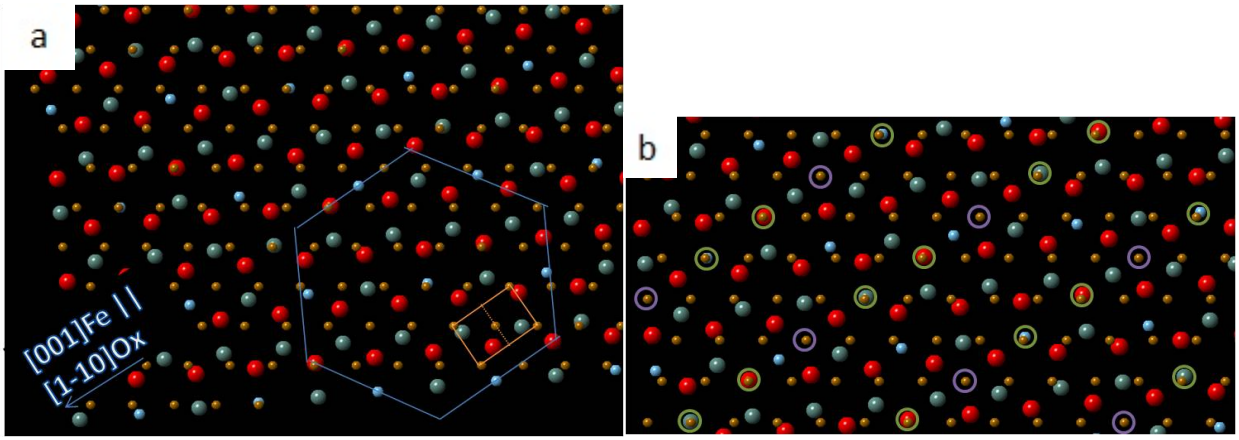

Figure 12. The orange, red, dark blue, and light blue circles are Fe, O, Y, and Ti, respectively. (a) The $\{1\text{-}10\}_{Fe}||\{111\}_{Y2Ti2O7}$ and $<001>_{Fe}||<1\text{-}10>_{Y2Ti2O7}$ OR. The blue hexagon in Figure 12a is the $\{111\}_{Y2Ti2O7}$ unit cell and the orange box is the $\{110\}_{Fe}$ unit cell. (b) Green circles show two well-matched Fe to substrate atoms and purple circles show Fe defect location.

Continuing and Future Research

This work is continuing and will be extended to other oxide surface orientations and different deposition conditions will also be explored. Another Fe deposition on $\{111\}_{Y2Ti2O7}$ was carried out with a deposition rate of 2 nm/s. Preliminary results show that there are Fe grains with one OR: $\{1\text{-}10\}_{Fe}||\{111\}_{Y2Ti2O7}$ and $<001>_{Fe}||<1\text{-}10>_{Y2Ti2O7}$. There were no Fe grains with {100} as seen in the sections above. The Fe grains had 3 in-plane orientations due to the 3-fold symmetry of the $Y_2Ti_2O_7$ {111} plane. This sample will be further characterized with AFM and HRTEM.

A Fe deposition was also done on a $\{001\}_{Y2Ti2O7}$ single crystal surface. The sample preparation and e-beam deposition conditions were kept the same as the previous deposits on $\{111\}_{Y2Ti2O7}$. XRD and EBSD scans show that only $\{110\}_{Fe}$ grains were seen and there was no in-plane OR with the substrate. This may be due to the non-stoichiometric termination of the $\{001\}_{Y2Ti2O7}$ plane, which made it difficult for the Fe grains to bond to the oxide surface. Further sample characterization will be carried out in the future.

There will also be studies of the interface interactions with irradiation induced defects and helium.

ACKNOWLEDGEMENTS

The authors thank Erin Haney, Gareth Seward, Mark Cornish, Deryck Stave, Youli Li, and Doug Klingensmith for help with various parts of the research. The work performed at UCSB was supported by the U. S. Department of Energy, Office of Fusion Energy Sciences, under grant DE-FG03-94ER54275. We also acknowledge the National Center for Electron Microscopy at LBL for the HRTEM on the TEAM 0.5 instrument in collaboration with Jim Cisten at LBL and Peter Hosemann at UC Berkeley.

REFERENCES

[1] G. R. Odette, M. J. Alinger, and B. D. Wirth, *Annu. Rev. Matter Res.* **38** (2008) 471
[2] Y. Dai, G. R. Odette, and T. Yamamoto, *Comp. Nucl. Mater.* **1** Chap. 6 (2012) 141
[3] H. Sakasegawa, L. Chaffron, F. Legendre, et al., *J. Nucl. Mater.* (2009) 384
[4] S. Yamashita, S. Ohtsuka, N. Akasaka, et al., *Phil. Mag. Lett.* (2004) 84
[5] S. Yamashita, N. Akasaka, and S. Ohnuki, *J. Nucl. Mater.* (2004) 329
[6] M. Klimiankou, R. Lindau, and A. Möslang, *J. Nucl Mater* (2004) 329
[7] M. Klimiankou, R. Lindau, and A. Möslang, *Micron* (2005) 36
[8] T. Okuda and M. Fujiwara, *J. Mater. Sci. Lett.* (1995) 14
[9] Y. Wu, E. M. Haney, N. J. Cunningham, et al., *Acta Mater.* **60** (2012) 3456
[10] J. Ciston, Y. Wu, G. R. Odette, et al., *Fus. Mat. Semiann. Prog. Rep.* (2012) DOE-ER-0313/51
[11] G. R. Odette, et al., *J. Nucl. Mater.* (2011)
[12] S. Y. Zhong, J. Ribis, V. Klosek, et al., *J. Nucl. Mater.* **12** (2012)
[13] M. J. Alinger, G. R. Odette, and D. T. Hoelzer, *J. Nucl. Mater.* (2004) 382
[14] J. S. Gardner, B. D. Gaulin, and D. M. Paul, *J. Cryst. Growth* **191** (1998) 740
[15] M. B. Johnson, H. A. Dabkowska, B. D. Gaulin, et al., *J. Solid State Chem.* **182** (2009) 725
[16] A. Hashibon, A. Y. Lozovoi, and P. Gumbsch, *Phys. Rev. B* **77** (2008) 094131